Low-energy NN tensor force from $\vec{n}$-$\vec{p}$ scattering: Results of an accurate experimental approach

J. R. Walston,[1,2,*] C. R. Gould,[1,2] D. G. Haase,[1,2] B. W. Raichle,[1,2,†] M. L. Seely,[1,2,‡] W. Tornow,[2,3] W. S. Wilburn,[2,3,§] S. I. Penttilä,[4] and G. W. Hoffmann[5]

[1]*Physics Department, North Carolina State University, Raleigh, North Carolina 27695*

[2]*Triangle Universities Nuclear Laboratory, Durham, North Carolina 27708*

[3]*Physics Department, Duke University, Durham, North Carolina 27708*

[4]*Los Alamos National Laboratory, Los Alamos, New Mexico 87545*

[5]*University of Texas, Austin, Texas 78712*

(Received 9 May 2000; published 18 December 2000)

The spin-dependent neutron-proton total cross-section differences $\Delta\sigma_L$ and $\Delta\sigma_T$ have been measured between $E_n=5$ and 20 MeV in longitudinal and transverse nucleon spin orientations. From these data the $^3S_1$-$^3D_1$ mixing parameter ε_1, which characterizes the nucleon-nucleon tensor force at low and intermediate energies, was determined in a model-insensitive way. In combination with measurements at higher energies, our values for ε_1 support a nucleon-nucleon tensor interaction that is stronger than predicted by all modern high-precision nucleon-nucleon potential models and phase-shift analyses.

DOI: 10.1103/PhysRevC.63.014004 PACS number(s): 25.40.Dn, 13.75.Cs, 24.70.+s, 25.10.+s

I. INTRODUCTION

A. Theoretical motivation

The quality with which the most recent nucleon-nucleon (NN) potential models [1–3] describe NN scattering data and the deuteron properties is remarkable. The NN database of the Nijmegen group [4] is reproduced with $\chi^2/N\approx 1$. However, if one uses these high-precision NN potentials to calculate the binding energy of ^{3}H, the simplest nontrivial nucleus, then one finds that both local and nonlocal potentials underbind ^{3}H by amounts ranging from 860 keV [1,2] to 480 keV [3]. Because the binding energy of few-nucleon systems is dominated by the contribution of the NN tensor force, which in turn is determined by the well-accepted one-boson exchange (OBE) mechanism, meson-exchange-based NN potential models seem destined to underbind all nontrivial nuclear systems.

Traditionally, the ^{3}H binding energy discrepancy is accounted for by adding phenomenological or semiphenomenological three-nucleon forces (3NF's). The inclusion of the 3NF's is justified at least at some level because the meson-exchange based NN potential models freeze out internal (i.e., quark) degrees of freedom. However, this approach is unsatisfactory for the ^{3}H binding energy problem unless NN and 3NF potentials are derived in an internally consistent way. This is the case only for the Ruhrpot potential [5].

Evidence for the importance of 3NF's in low-energy scattering processes is also subject to criticism. It is known that agreement between the rigorously calculated $^2S_{1/2}$ phase shift in $p+d$ scattering and the result obtained from $p+d$ phase-shift analyses can be improved by adding a 3NF adjusted to fit $E_{^3\mathrm{H}}^{exp}$ [6]. However, this observation does not prove the existence of a sizable 3NF, because it can be argued, as in the case of the bound state, that the central part of the NN potential is not sufficiently strong. A stronger central force is readily accomodated in meson-exchange based NN potential models if the tensor force is made weaker to match the deuteron binding energy. The evidence for the importance of 3NF's therefore rests on the assumption that the well-understood OBE is largely responsible for the NN tensor force, and that OBE is indeed the correct effective description of the underlying theory, quantum chromodynamics (QCD). Before calling for 3NF's, it is critical to learn whether NN potential models do in fact describe low-energy, tensor-force related NN observables to the necessary accuracy.

Beyond interest in the existence of 3NF's, there is renewed theoretical interest in how best to describe both the long-range (one-boson exchange) and the short-range (six-quark) characteristics of the NN interaction using the same formalism. Hybrid-type NN potential models [7] take into account meson and quark degrees of freedom in different frameworks, which give rise to interesting interference phenomena between the tensor and the central force. In the constituent quark model, obtained in a nonrelativistic limit from the QCD Lagrangian, the NN interaction is described by a six-quark wave function consisting of the two-nucleon clusters and a Hamiltonian acting on the quarks [8]. The Hamiltonian includes a σ-meson exchange potential on the nucleon level. Finally, in Weinberg's approach [9] the starting point is the most general Lagrangian in terms of pion and nucleon fields and their covariant derivatives, incorporating the approximate chiral symmetry of QCD. Corrections to the one-pion exchange (OPE) potential arise naturally and are taken into account [10,11].

*Present address: Magma Design Automation, Durham, NC 27713.

†Present address: Department of Physics and Astronomy, Appalachian State University, Boone, NC 28608.

‡Present address: Thomas Jefferson National Accelerator Facility, Newport News, VA 23606.

§Present address: Los Alamos National Laboratory, Los Alamos, NM 87545.

With these ongoing theoretical activities in mind it is important to measure specific *NN* parameters which are, in the conventional meson-exchange descriptions, governed by the exchange of only a small number of bosons. Only with accurate data for these parameters will it be possible to distinguish between the traditional and the recent more fundamental approach to the *NN* interaction and to discern whether the description of the ^{3}H binding energy indeed requires sizeable 3NF's.

An excellent test case for probing the accuracy of the OBE mechanism is the comparison of experimental data and *NN* potential model predictions for the $^3S_1$-$^3D_1$ mixing parameter ε_1 in neutron-proton $(n+p)$ scattering. The phase shift ε_1 is a measure of the *NN* tensor force at low energies. In OBE potential models the magnitude of the tensor force results from the interplay of an attractive OPE contribution and the repulsive ρ-exchange contribution [12]. The appropriate balance between these two contributions is mainly obtained from fits to the $^3P_0$ and $^3P_2$ *NN* phase-shift parameters at energies above 100 MeV. Therefore, the effective tensor force used in OBE potential models is not based on the deuteron properties and low-energy *NN* data alone, but is crucially influenced by higher energy phenomena [12]. In practice, it is important to directly compare to data rather than to phase-shift descriptions of ε_1, because phase-shift analyses traditionally incorporate OPE as a tool for obtaining unique phase-shift solutions. The parameter ε_1, as well as all other *NN* parameters, cannot be determined in a direct sense through a single experiment. In general, its determination requires the knowledge of other *NN* phase-shift parameters.

In this paper we present the results of a powerful experimental approach for determining ε_1 which minimizes the sensitivity to other *NN* parameters, thereby allowing an accuracy in the determination of ε_1 that has not been achieved previously. The measurements consist of transverse and longitudinal cross-section differences for polarized neutron scattering from polarized protons in the 5 to 25 MeV energy range. Our results were published in short form in Ref. [13].

B. Previous status of ε_1 at low energies

To obtain information about the accuracy of the OBE mechanism, high-accuracy determinations of the isospin $T=0$, $^3S_1$-$^3D_1$ mixing parameter ε_1 are required at low energies. For the ^{3}H binding energy problem, nucleon energies up to about 60 MeV are important. The knowledge of ε_1 in this energy range prior to the present TUNL results is summarized in Fig. 1.

The datum at $E_n=50$ MeV is based mainly on backward-angle data for the spin-correlation coefficient $A_{zz}(\theta)$ in $\vec{n}+\vec{p}$ scattering obtained at PSI [14]. The Bonn value at 25.8 MeV determined from a polarization-transfer coefficient $D_t(\theta)$ measurement $(\vec{n}+p\rightarrow n+\vec{p})$ at $\theta_{\rm c.m.}=123°$ [15] agrees with the trend of the PSI result. However, the value obtained by the Bonn group at 17.4 MeV (open circle) in a similar experiment (using neutrons from the reactions ^{2}H$(d,np)^2$H and ^{2}H$(d,npnp)$ rather than ^{2}H$(d,n)^3$He) [16] is considerably lower, and agrees with the datum (square) of the Erlangen/Tübingen group [17]. The Bonn group has recently confirmed its previous result [18] in an experiment using $E_n=17.4$ MeV neutrons from the ^{2}H$(d,n)^3$He reaction.

On the other hand, the recent measurements by the Prague/Dubna group (open triangle in Fig. 1) at the nearby energy of $E_n=16.1$ MeV [19,20] are in excellent agreement with theoretical expectations and nicely follow the trend of the 1995 TUNL data of Wilburn *et al.* [21] at energies below 11.6 MeV (shown as filled triangles). The 13.7 MeV Erlangen/Tübingen result [17] was obtained from a measurement of the spin-correlation coefficient $A_{yy}(\theta)$ in $\vec{n}+\vec{p}$ scattering at $\theta_{\rm c.m.}=90°$. The TUNL data [21] are based on measurements of the $\vec{n}+\vec{p}$ transverse total cross-section difference $\Delta\sigma_T$, whereas the recent Prague/Dubna determinations [19,20] of ε_1 were obtained from measurements of both the transverse [19] and longitudinal [20] $\vec{n}+\vec{p}$ total cross-section difference $\Delta\sigma_T$ and $\Delta\sigma_L$. It remains a mystery why the ε_1 values of both the Erlangen/Tübingen group at $E_n=13.7$ MeV and of the Bonn group at $E_n=17.4$ MeV are so small compared to theoretical expectations shown in Fig. 1. Here, the solid curve represents the result of the Nijmegen Partial-Wave Analysis PWA93 [4], which is in close agreement with the Bonn B *NN* potential-model description [22] given by the dashed curve. The dashed-dotted curve is the VPI phase-shift analysis result (FA95) [23]. This curve is different from the other representations of ε_1, but it describes the experimental values of ε_1 considerably better in the energy range above 20 MeV. Not shown, but almost indistinguishable from the solid curve are the Nijmegen (Nijm93) [1], Argonne AV18 [2], and CD-Bonn [3] *NN* potential-model predictions. This observation is not too surprising since these three potential models are fitted to PWA93 [4].

Summarizing Fig. 1, it is obvious that only the phase-shift analysis of the VPI group is in reasonably good agreement with the data at energies above 20 MeV.[1] OPE-based theoretical constraints prevent both the Nijmegen PWA93 and the *NN* potential models from reproducing these data. The relatively steep slope of ε_1 at very low energies is related to the quadrupole moment of the deuteron. Starting at energies above 10 MeV, theory predicts a decreased energy dependence of ε_1. If the two determinations of ε_1 at $E_n=25.8$ and 50 MeV are indeed correct, then either the balance between OPE and ρ exchange is not correctly adjusted in the present *NN* potential models, or other, currently unknown physics contributes to the *NN* tensor force in the energy range of interest.

II. POLARIZED NEUTRON-POLARIZED PROTON TOTAL CROSS-SECTION DIFFERENCES

As seen from Sec. I B, the determination of ε_1 from $n+p$ scattering requires at least two polarization measure-

[1]In Fig. 1 we did not include the results of the Karlsruhe group [24] obtained from $A_{yy}(\theta)$ meaurements between 20 and 50 MeV due to the relatively large fluctuations present in these data. They are included in the VPI analysis, but not in the Nijmegen PWA93 analysis. On the average, the Karlsruhe results are above the VPI curve.

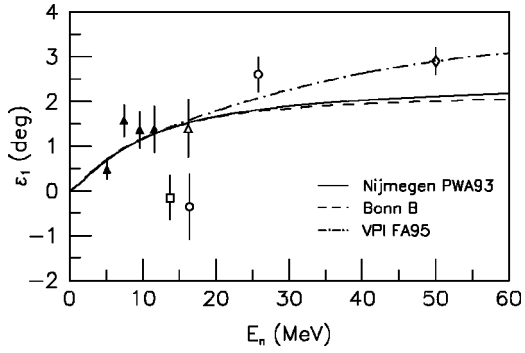

FIG. 1. Experimentally determined values of the phase-shift parameter ε_1 and theoretical predictions prior to our present work. References are given in the text.

ments. Either a polarized neutron beam and a polarized proton target are required, or, if only one of the two particles in the entrance channel is polarized, then the polarization of at least one of the two particles in the exit channel must be measured. From all the possible observables in the $n+p$ scattering system which meet these requirements, spin-dependent total cross-section difference measurements are experimentally the most attractive ones for determining ε_1. We will show that they are also extremely attractive from a theoretical point of view.

The spin-dependent total cross-section differences are defined as the differences in the total cross sections with the proton target and neutron beam polarized antiparallel and parallel to each other and directed either longitudinal (L) or transverse (T) to the beam direction:

$$\Delta\sigma_L=\sigma(\rightleftarrows)-\sigma(\rightrightarrows), \tag{1}$$

$$\Delta\sigma_T=\sigma(\uparrow\downarrow)-\sigma(\uparrow\uparrow), \tag{2}$$

where the top (first) arrow refers to the proton target and the bottom (second) arrow to the neutron beam spin orientations.

For particles with spin, the optical theorem relates the total cross section σ_t to the forward scattering amplitude $f'_{m'M',mM}(0°)$ by [25]

$$\sigma_t=4\pi\lambda\!\!\!^{-}Im\left\{\sum_{mm'}\sum_{MM'}\rho_{mm'}\rho_{MM'}f'_{m'M',mM}(0°)\right\}, \tag{3}$$

where $\rho_{mm'}$ and $\rho_{MM'}$ are the density matrices of the projectile and target, respectively, and $\lambda\!\!\!^{-}$ is the reduced wavelength. Following Hnizdo [26,27], the total cross section can be written in terms of partial cross sections $\sigma_{kK\Lambda}$ corresponding to different ranks k and K of the statistical tensors of the beam and target, respectively, and to different values of the transfered orbital angular momentum Λ. For a spin $s=\frac{1}{2}$ neutron incident on a spin $I=\frac{1}{2}$ proton, the result is

$$\sigma_t=\sigma_0+P\sigma_1, \tag{4}$$

where $\sigma_0\equiv\sigma_{000}$ is the spin-independent part of the cross section and σ_1 is the spin-dependent part of the cross section, consisting of central and tensor terms σ_{110} and σ_{112}, respectively [26],

$$\sigma_1=\left\{\sqrt{\frac{1}{3}}(\hat{\mathbf{s}}\cdot\hat{\mathbf{I}})\sigma_{110}+\sqrt{\frac{3}{10}}\left[(\hat{\mathbf{s}}\cdot\hat{\mathbf{p}})(\hat{\mathbf{I}}\cdot\hat{\mathbf{p}})-\frac{1}{3}\hat{\mathbf{s}}\cdot\hat{\mathbf{I}}\right]\sigma_{112}\right\}P_T. \tag{5}$$

In Eqs. (4) and (5) P is the polarization of the neutron beam, P_T is the polarization of the proton target, $\hat{\mathbf{s}}$ and $\hat{\mathbf{I}}$ are unit vectors in the directions of the neutron and proton spin, respectively, $\hat{\mathbf{p}}$ is a unit vector in the direction of the neutron beam. The transverse and longitudinal cross-section differences are given by

$$\Delta\sigma=-\frac{2\sigma_1}{P_T} \tag{6}$$

with σ_1 evaluated for the respective geometries $\hat{\mathbf{s}}$, $\hat{\mathbf{I}}$, and $\hat{\mathbf{p}}$. To evaluate the asymmetry in transmission due to $\Delta\sigma$, we consider the transmission of neutrons through a target layer dx. The change in flux is given by

$$dN^{\pm}=-N^{\pm}(\sigma_0\pm\sigma_1)dx, \tag{7}$$

where $N^{\pm}$ is the number of neutrons in the magnetic spin substate $m=\pm1/2$. Differences in attenuation for the two spin states lead to a change in beam polarization P, given by

$$\frac{1}{\sigma_1}\frac{dP}{dx}-P^2+1=0. \tag{8}$$

Solving Eq. (8) for the initial condition $P(x=0)=P_n$ gives the polarization as a function of target thickness x:

$$P(x)=\frac{P_n-\tanh(x\sigma_1)}{1-P_n\tanh(x\sigma_1)}. \tag{9}$$

The change in the total number of neutrons $N=N^+ +N^-$ is now given by

$$dN=-N[\sigma_0+P(x)\sigma_1]dx, \tag{10}$$

which can be integrated to give the total number of neutrons N after passing through a thickness x:

$$N=N_0e^{-\sigma_0x}[\cosh(\sigma_1x)-P_n\sinh(\sigma_1x)], \tag{11}$$

where N_0 is the number of neutrons incident on the target. The asymmetry ϵ_n of the transmitted neutrons is given by

$$\epsilon_n=\frac{N(+P_n)-N(-P_n)}{N(+P_n)+N(-P_n)}=-P_n\tanh(\sigma_1x). \tag{12}$$

Since the argument of the hyperbolic tangent is less than 0.05 for neutron energies above 1 MeV, this can be approximated by

$$\epsilon_n\simeq-P_n\sigma_1x. \tag{13}$$

Finally, using this relation and Eq. (6), we obtain for the cross-section difference

$$\Delta\sigma=\frac{2\epsilon_n}{P_nP_Tx}. \tag{14}$$

In terms of *NN* phase-shift parameters, $\Delta\sigma_L$ and $\Delta\sigma_T$ are given by

$$\Delta\sigma_L=\frac{\pi}{k^2}\{2-\cos 2\delta(^1S_0)-\cos 2\delta(^3P_0)+3[\cos 2\delta(^3P_1)-\cos 2\delta(^1P_1)]$$
$$+\cos 2\varepsilon_1[\cos 2\delta(^3S_1)-\cos 2\delta(^3D_1)]+5[\cos 2\delta(^3D_2)-\cos 2\delta(^1D_2)]$$
$$+\cos 2\varepsilon_2[\cos 2\delta(^3P_2)-\cos 2\delta(^3F_2)]+4\sqrt{2}\sin[\delta(^3S_1)+\delta(^3D_1)]\sin 2\varepsilon_1$$
$$+4\sqrt{6}\sin[\delta(^3P_2)+\delta(^3F_2)]\sin 2\varepsilon_2\}, \tag{15}$$

$$\Delta\sigma_T=\frac{\pi}{k^2}\{\cos 2\delta(^3P_0)-\cos 2\delta(^1S_0)-3\cos 2\delta(^1P_1)+\cos 2\varepsilon_1[\cos 2\delta(^3S_1)+2\cos 2\delta(^3D_1)]$$
$$-5\cos 2\delta(^1D_2)+\cos 2\varepsilon_2[2\cos 2\delta(^3P_2)+3\cos 2\delta(^3F_2)]$$
$$-2\sqrt{2}\sin[\delta(^3S_1)+\delta(^3D_1)]\sin 2\varepsilon_1-2\sqrt{6}\sin[\delta(^3P_2)+\delta(^3F_2)]\sin 2\varepsilon_2\}, \tag{16}$$

where k is the wave number and the phase shifts δ are labeled in spectroscopic notation $\delta(^{2S+1}L_J)$. Terms with $J\geqslant 3$ are omitted because they contribute negligibly to $\Delta\sigma_L$ and $\Delta\sigma_T$ in the energy range of interest. The large sensitivity of $\Delta\sigma_L$ and $\Delta\sigma_T$ to ε_1 at low energies is due to cancellations between individual phase shifts. Figures 2(a) and 2(b) show the sensitivity of $\Delta\sigma_T$ and $\Delta\sigma_L$ to a $\pm 1°$ variation of ε_1 in the energy range below $E_n=25$ MeV, the energy range of interest in the present work. Here, we started from the Nijmegen PWA93 result, shown as a solid curve, and increased (decreased) ε_1 by 1° and obtained the dashed-dotted (dashed) curve. Note also that the sensitivity of $\Delta\sigma_L$ to variations of ε_1 is a factor of 2 larger than that for $\Delta\sigma_T$. It is also important to point out that there is a considerable loss in sensitivity with increasing neutron energy.

As has been pointed out in Refs. [21,28], an even larger sensitivity to ε_1 can be obtained by introducing the observable

$$\Delta=\Delta\sigma_L-\Delta\sigma_T=\frac{\pi}{k^2}\{2-2\cos 2\delta(^3P_0)+3\cos 2\delta(^3P_1)+5\cos 2\delta(^3D_2)$$
$$-3\cos 2\varepsilon_1\cos 2\delta(^3D_1)-[\cos 2\delta(^3P_2)+4\cos 2\delta(^3F_2)]\cos 2\varepsilon_2$$
$$+6\sqrt{2}\sin[\delta(^3S_1)+\delta(^3D_1)]\sin 2\varepsilon_1+6\sqrt{6}\sin[\delta(^3P_2)+\delta(^3F_2)]\sin 2\varepsilon_2\}. \tag{17}$$

In contrast to $\Delta\sigma_T$ and $\Delta\sigma_L$, the difference Δ does not depend on any singlet *NN* phase shifts. This reduces the model dependence in the determination of ε_1 to a minimum and at the same time maximizes its sensitivity to ε_1. Figure 2(c) shows the dramatic sensitivity of the observable Δ to a $\pm 1°$ variation of ε_1. Again, this sensitivity is due to cancellations between the different terms given in Eq. (17). For example, inserting the PWA93 phase shifts at $E_n=12$ MeV into Eq. (17) (except for the $\sin 2\varepsilon_1$ term) one obtains

$$\Delta=\frac{\pi}{k^2}\{8.41\sin 2\varepsilon_1+0.01\}. \tag{18}$$

III. EXPERIMENTAL SETUP

The experimental determination of $\Delta\sigma_L$ ($\Delta\sigma_T$) requires the measurement of the transmission asymmetry for a longitudinally (transversely) polarized neutron beam through a longitudinally (transversely) polarized proton target when one or the other spin is reversed. Following Eq. (14), the product of proton target polarization and thickness ($P_T x$) and the neutron polarization P_n must be known accurately in order to determine $\Delta\sigma_L$, $\Delta\sigma_T$ and Δ from the measured asymmetry ϵ_n. Data for $\Delta\sigma_L$ were obtained at neutron energies of 4.98, 6.95, 10.72, 14.65, 17.14, and 19.71 MeV. The previous data set for $\Delta\sigma_T$ of Wilburn *et al.* [21] between 3.65 and 11.60 MeV was extended to higher energies. Data were taken at neutron energies of 10.70, 14.58, and 17.08 MeV.

A schematic diagram of the experimental setup is shown in Fig. 3. A polarized neutron beam in the 2 to 20 MeV energy range is produced by charged-particle reactions in the neutron production target. The zero-degree neutron flux is monitored by a small transmission-type monitor detector which is attached to a phototube (not shown) via a long light guide. The polarized proton target is centered in a superconducting magnet and the transmitted neutrons are detected in the shielded zero-degree neutron detector located at the end of a collimator. In the following sections we will briefly describe the parts of the experimental setup that are crucial for an accurate determination of $\Delta\sigma_L$ and $\Delta\sigma_T$.

A. The polarized proton target

In contrast to the statically polarized proton target (TiH_2) used in previous TUNL measurements [21], the present tar-

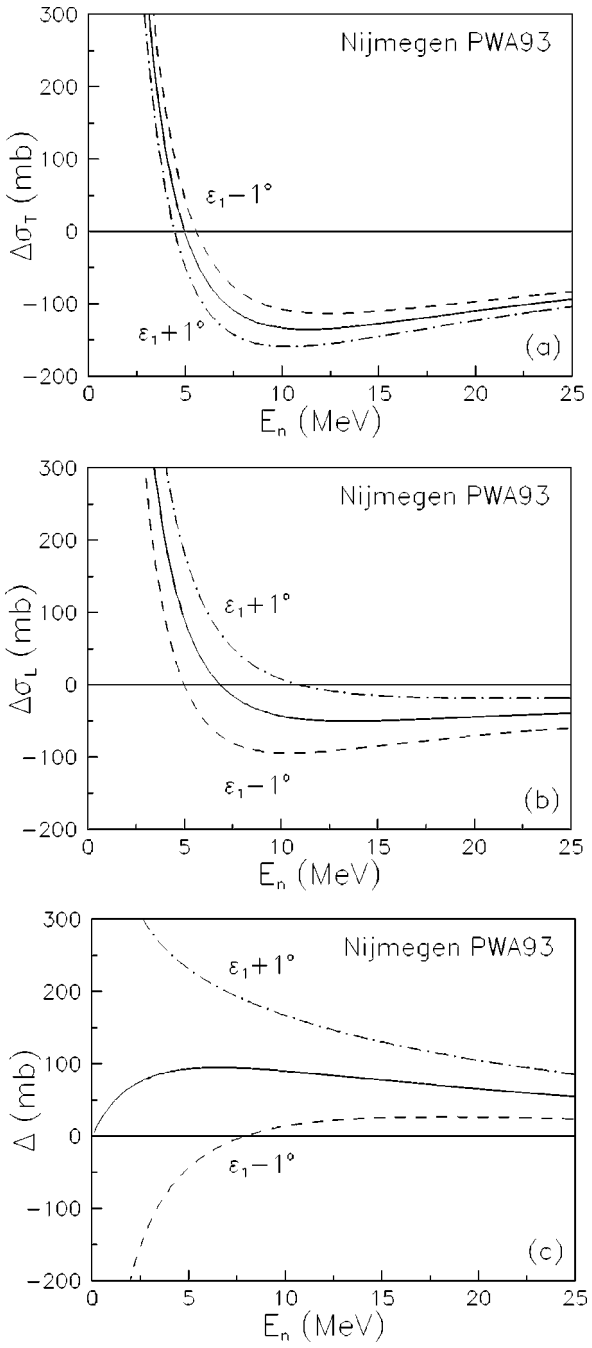

FIG. 2. Sensitivity of $\Delta\sigma_T$ (a), $\Delta\sigma_L$ (b), and Δ (c) to $+1°$ (dot-dashed curve), and $-1°$ (dashed curve) variations in ε_1 at neutron energies $E_n=25$ MeV. The solid curve is from the Nijmegen PWA93 analysis.

get is dynamically polarized [29]. Dynamic polarization allows for a rapid reversal ($\approx$30 min) of the polarization direction of the target, which is crucial for canceling the effect of instrumental asymmetries. In a transmission experiment the figure of merit of a polarized target is $(P_T x)^2$, the square of the polarization P_T times thickness x, stressing the need for both high polarization and high density.

The target material is 1,2 propanediol [$C_3H_6(OH)_2$, density 1.27 g/cm^3], frozen into 1 mm diameter beads, giving a hydrogen concentration of 5×10^{22} H/cm^3. The propanediol is chemically doped with 2-ethyl 2-hydroxybutyric acid (EHBA) in a complex with chromium-V [30] to provide the free electrons (4×10^{19} electrons/cm^3) required for dynamic nuclear polarization (DNP). The target thickness is nominally 0.06 H/barn (compared to 0.02 H/barn of our previous TiH_2 based polarized proton target). The target is cooled to 0.5 K by a ^{3}He evaporation refrigerator of the PSI design [31]. DNP was induced using a microwave system and superconducting magnet.

A schematic view of the cryostat is shown in Fig. 4. The ^{4}He dewar and the liquid-^{4}He-filled split-coil superconducting magnet are surrounded by a vacuum jacket, two copper heat shields and several layers of aluminized mylar. The dewar is cooled to 2 K by pumping on the ^{4}He bath which is in thermal contact with a ^{3}He condenser where recirculating ^{3}He gas condenses.

The ^{3}He refrigerator (shown in Fig. 5) cools the target to 0.5 K by pumping on ^{3}He. At this temperature the cooling power of the refrigerator is approximately 15 mW with a ^{3}He flow rate of 0.6 mmol/s. The ^{3}He system is modular in construction and is top loaded into the cryostat, making it independent from the ^{4}He system. At the bottom of the refrigerator is the ^{3}He cup. Liquid ^{3}He fills this cup and immerses the target cup, a $1.4\times1.4\times1.4$ cm^3 (inner dimensions) container. The target cup is fastened to the microwave horn located at the end of a long target insert (Fig. 5), which is top loaded into the center bore of the refrigerator. The target insert is also the microwave waveguide from room-temperature to 0.5 K, and supports the NMR coaxial cable. Figure 6 gives details of the target cup seated in the ^{3}He cup.

The free electrons provided by chemical doping are nearly 100% polarized at 0.5 K and 2.6 T. Nuclear polarization is induced by pumping with $\approx$7 mW of microwave radiation at 69.524 GHz for positive and 69.124 GHz for negative proton polarization [29].

NMR measurements were made continuously to monitor the relative proton target polarization during the $\Delta\sigma_T$ and $\Delta\sigma_L$ experiments and during the absolute $P_T x$ calibration measurements at low neutron energies. Typically, the target polarization was $P_T=65\%$. The NMR system was calibrated by measurement of the thermal equilibrium proton target polarization at 0.5 and 1.0 K before each $\Delta\sigma$ measurement. The NMR coil is made of two loops of 0.051 cm diameter copper wire wrapped around the outside of the target cup, as shown in Fig. 7. The coil is connected to room-temperature electronics by a cryogenic coaxial cable. The LRC circuit response is measured by a Liverpool box [32] tuned to the proton Larmor frequency. Measurements of the circuit response with the magnet tuned off-resonance (unpolarized) were also made for background subtraction.

B. The polarized neutron beam

The polarized neutron beam was produced as a secondary beam using one of four different neutron-production reactions: transverse and longitudinal polarization transfer in the ^{3}H$(\vec{p},\vec{n})^3$He reaction at low energies to calibrate the product of $P_T x$ for the polarized proton target, and transverse and

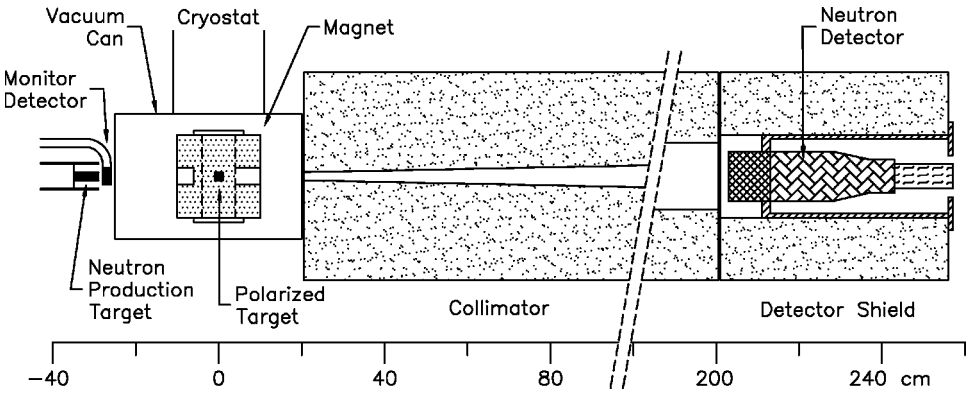

FIG. 3. Schematic of the experimental setup showing the neutron production target attached to the beamline, neutron monitor detector, polarized target, collimator, and zero-degree neutron detector.

longitudinal polarization transfer in the $^2\mathrm{H}(\vec{d},\vec{n})^3\mathrm{He}$ reaction to measure $\Delta\sigma_T$ and $\Delta\sigma_L$ at the energies of interest.

The polarized proton or deuteron beam was produced by the TUNL Atomic Beam Polarized Ion Source [33] and the TUNL 10 MV tandem Van de Graaff accelerator. A Wien Filter was used to produce the desired quantization axis (transverse or longitudinal) on target.

The target for low-energy ($E_n<2$ MeV) neutron production consisted of a 2.2 mg/cm^2 layer of tritiated titanium ($\approx \mathrm{TiT}_{1.4}$) evaporated onto a metallic beam stop. Proton beam currents were typically 1 μA and beam energies were 2.95 MeV (transverse) or 1.83 MeV (longitudinal). The neutron beam energy was determined by observing $n-{}^{12}\mathrm{C}$ cross-section resonances. The proton beam polarization was determined from measurements of left/right scattering asymmetries in $p-{}^4\mathrm{He}$ scattering (see Sec. IV B1). The quantization axis of the beam was precessed transverse at the Wien Filter for polarimetry during the $\Delta\sigma_L$ measurements. The neutron beam polarization was then calculated from the proton beam polarization and from the polarization-transfer coefficients (see Sec. IV B 3).

The target for high-energy ($E_n>5$ MeV) neutron production was a 6.0 cm long deuterium gas cell separated from the beamline vacuum by a 6.4×10^{-4} cm thick Havar window and terminated by a metallic beamstop. The cell was filled to 3×10^5 Pa and beam currents were typically 1 μA. The deuteron beam polarization was determined from measurements

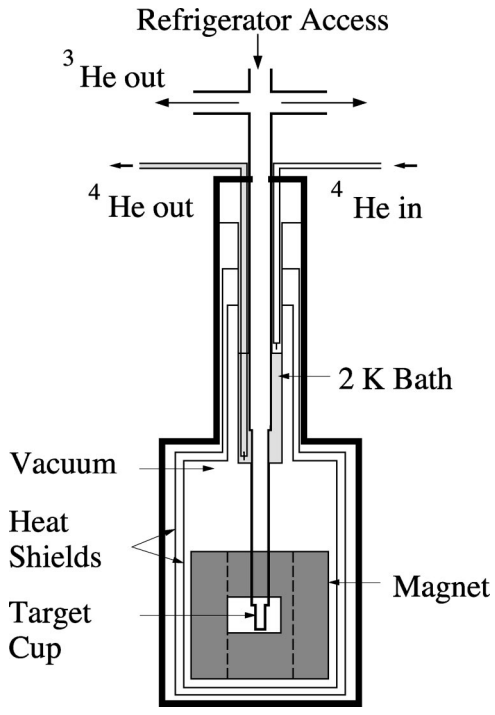

FIG. 4. Schematic of the ^{4}He cryostat. The superconducting magnet gets liquid ^{4}He from the 2 K bath through two small bellows (not shown).

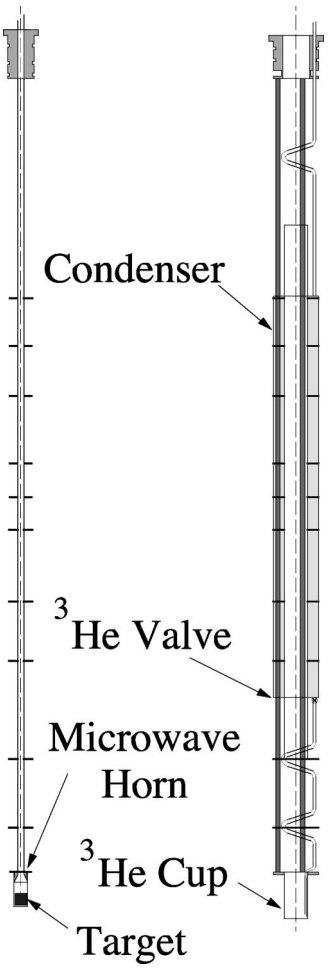

FIG. 5. Schematic of the target insert and ^{3}He fridge. The fridge and insert can be top loaded into the cold cryostat [31].

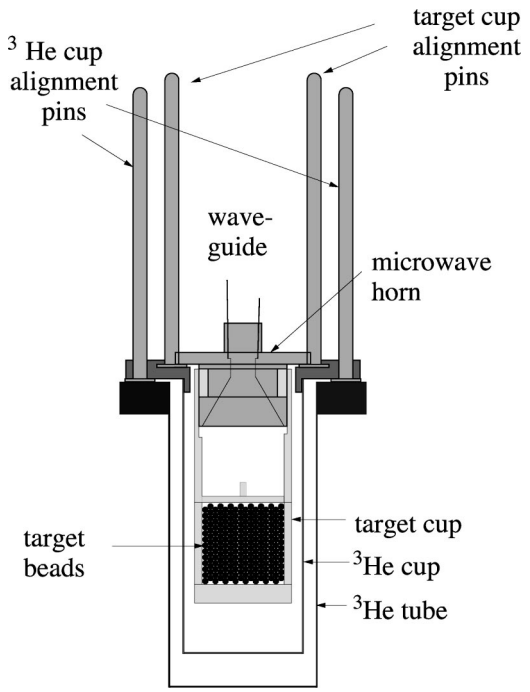

FIG. 6. Schematic of the ^{3}He cup inserted into the refrigerator.

of left/right scattering asymmetries from the $^3\mathrm{He}(\vec{d},p)^4\mathrm{He}$ reaction (see Sec. IV B 2). As for protons, the quantization axis of the beam was precessed transverse at the Wien Filter for polarimetry during the $\Delta\sigma_L$ measurements. The neutron beam polarization was calculated from measured deuteron beam polarizations and known polarization-transfer coefficients (see Sec. IV B 3).

C. Neutron detectors

Two neutron detectors were used in the present experiment: a monitor detector and a zero-degree neutron detector (see Fig. 3). These detectors are described below.

The monitor detector is described in Wilburn *et al.* [21], with the exception that a transistorized base [34] was used to reduce count-rate-dependent gain changes [35]. The detector was placed in the neutron beam downstream of the neutron production target (see Fig. 3) and coupled to a phototube via a 1 m long light pipe. This geometry places the phototube outside of the fringe field of the superconducting magnet of our polarized proton target. The monitor detector was used only for the runs where the polarized neutron beam was produced by the $^2\mathrm{H}(\vec{d},\vec{n})^3\mathrm{He}$ reaction. In this case the neutron yield is weakly dependent on the deuteron beam tensor polarization, so beam current integration alone is not sufficient to determine the neutron flux incident on the polarized proton target.

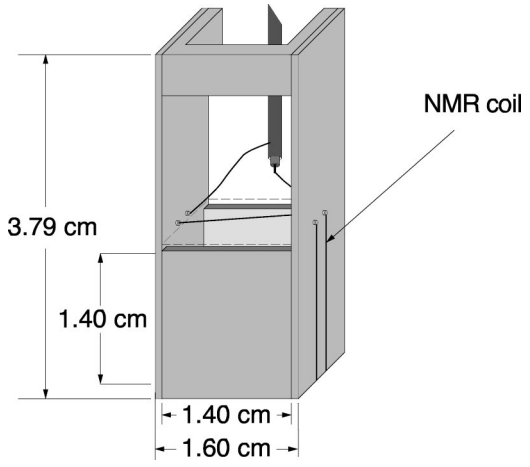

FIG. 7. Schematic of the target cup showing the NMR coil.

The zero-degree neutron detector consisted of a 12.7 cm diameter$\times$12.7 cm long organic scintillator (Bicron 501) attached to a photomultiplier tube which was coupled to a transistorized base. The detector was mounted inside a polyethylene collimator used to define the neutron beam viewed by the detector. The collimator prevents room scattered neutrons from reaching the neutron detector. The entrance bore of the collimator was located 45.7 cm from the neutron production target, and 18.4 cm from the polarized proton target. The bore was 2.4 cm$\times$2.4 cm with a taper to 9 cm$\times$9 cm at the exit of the 128.3 cm long collimator (2.5 msrad solid angle). The distance between the zero-degree neutron detector (polarized proton target) and the neutron-production target was 211.5 cm (238.8 cm). The alignment of the polarized proton target with respect to the neutron beam was verified at 77 K by placing a small copper block with a small centered alignment hole in the target cup and then exposing an x-ray film at the exit of the collimator. The γ-ray flux in the beam was sufficient to expose the film (for 20 min) and to show clearly the position of the hole in the copper block.

IV. MEASUREMENT PROCEDURES

A. Neutron transmission asymmetry measurements

As stated earlier, transverse asymmetries were measured at $E_n=10.70$, 14.58, and 17.08 MeV, and longitudinal asymmetries were measured at 4.98, 6.95, 10.72, 14.65, 17.14, and 19.71 MeV. In addition, transmission asymmetries were measured at low energy [$E_n=1.92$ MeV ($\Delta\sigma_T$) and $E_n=0.79$ MeV ($\Delta\sigma_L$)] to calibrate the product $P_T x$. The same experimental and analysis procedures were followed in all neutron asymmetry measurements. The beam polarization was reversed at 10 Hz in the eight-step sequence $+--+-++-$ to minimize sensitivity to drifts in time to second order [36], and the target polarization was reversed every 4–6 h. The measured neutron asymmetries ranged in magnitude from 0.2×10^{-4} to 400×10^{-4}. The statistical uncertainty was typically less than 1% after 24 h of data taking.

The neutron yields were normalized to the integrated beam current when the polarized neutron beam was produced by the $^3\mathrm{H}(\vec{p},\vec{n})^3\mathrm{He}$ reaction. When the polarized neutron beam was produced by the $^2\mathrm{H}(\vec{d},\vec{n})^3\mathrm{He}$ reaction, the measured neutron yields were normalized to the monitor detector yields. This normalization accounts for a beam-current asymmetry as well as for a neutron flux asymmetry due to the tensor polarization dependence of the source reaction [45].

The signals from the zero-degree neutron detector were analyzed using pulse-shape discrimination in order to separate neutron events from γ-ray events. A high threshold was set to remove breakup neutron events from the monoenergetic ^{2}H$(d,n)^3$He events. The threshold settings were verified in separate measurements with a pulsed beam and neutron time-of-flight techniques. The high count rate in the monitor detector precluded the use of pulse-shape discrimination. Instead, we relied on a high-threshold setting and the low detector efficiency for γ rays in this very small scintillator. Events from the zero-degree and monitor detectors, as well as beam current and dead-time information, were recorded and tagged with spin orientation and recorded on a spin-flip (800 ms) basis.

In practice, the measurement of a transmission asymmetry is susceptible to many systematic effects. In addition to asymmetries due to incident neutron flux asymmetries, we considered effects resulting from dead-time asymmetries and false asymmetries due to count-rate dependent detector efficiencies. The correction procedures are discussed in more detail in Refs. [13,36,37]. The main systematic error arises from a nonlinear neutron detector efficiency, which contributed to a false asymmetry typically of order 10% of the measured asymmetry. Uncertainty in this correction was treated as systematic and added in quadrature to the statistical uncertainty for subsequent calculations.

B. Beam polarization measurements

The charged-particle beam polarization was determined from analyzing reactions in a polarimeter chamber [37] located some 5 m in front of the polarized target. The polarimeter consisted of a 2.54 cm diameter$\times$3.81 cm high gas cell made of 2.29×10^{-4} cm Havar foil which was inserted into the beam for polarimetry. Feedback slits immediately in front of the chamber were adjusted to form a 4 mm$\times$4 mm aperture. Charged particles were detected by three collimated silicon detectors. One of the detectors was placed at zero degrees (with an appropriate stopping foil in front) and the other two were placed symmetrically to the left and to the right of the beam propagation axis. Events from the three detectors were tagged for routing with detector and spin-state information. The neutron beam polarization was calculated from the measured charged-particle polarizations and polarization-transfer coefficients.

1. Proton beam polarimetry

The proton beam polarization was determined from the measured left/right asymmetry in $p-^4$He elastic scattering. The proton beam polarization is given by

$$P_p=\frac{\epsilon_p}{A_y}, \tag{19}$$

where A_y is the $p-^4$He analyzing power, which in general depends on incident beam energy and angle. A_y was calculated from the partial-wave expansion of the elastic scattering amplitude for spin-$\frac{1}{2}$ particles given by Satchler [38]. Phase shifts were taken from the effective-range parametrization of Schwandt [39]. The asymmetry was calculated from

$$\epsilon_p=\frac{\left(\frac{N_{L+}N_{R-}}{N_{L-}N_{R+}}\right)^{1/2}-1}{\left(\frac{N_{L+}N_{R-}}{N_{L-}N_{R+}}\right)^{1/2}+1} \tag{20}$$

to cancel detector efficiencies. The $N_{\alpha\beta}$ are counts in the α detector for the β spin state.

The detectors were positioned at the angle of greatest analyzing power for maximum sensitivity ($\theta_{lab}=111°$ for transverse measurements at $E_p=2.95$ MeV, $\theta_{lab}=81°$ for longitudinal measurements at $E_p=1.83$ MeV). The analyzing gas cell was filled to 10^5 Pa of ^{4}He gas.

The asymmetries were analyzed on a channel-by-channel basis. A statistical uncertainty of $<1\%$ was obtained in ≈5 min. The proton beam polarization was measured approximately every 4 h during each low-energy $\Delta\sigma$ measurement to calibrate P_Tx for each target. Typical values for the proton beam polarization were of order 70%.

2. Deuteron beam polarimetry

Deuteron-beam polarimetry was performed using the ^{3}He$(\vec{d},p)^4$He reaction at $E_d=8.0$ MeV during the $\Delta\sigma_T$ measurements, and at $E_d=8.0$ or 12.0 MeV during the $\Delta\sigma_L$ measurements. The polarimeter side detectors were positioned at the angle of maximum iT_{11} ($\theta_{lab}=111°$ for measurements at $E_d=8.0$ MeV, $\theta_{lab}=130°$ for measurements at $E_d=12.0$ MeV). The gas cell was filled to 10^5 Pa of ^{3}He gas.

Both polarized and unpolarized data were taken. The vector and tensor deuteron beam polarizations were calculated from zero-degree detector normalized, left/right detector yields for both polarized and unpolarized beam. The zero-degree flux was measured by the zero-degree charged-particle detector ($\Delta\sigma_T$ measurements) or by the neutron-monitor detector ($\Delta\sigma_T$ measurements).

The ^{3}He$(\vec{d},p)^4$He analyzing powers iT_{11}, T_{20}, and T_{22} were obtained from Legendre polynomial fits to phase shifts taken from Bittcher *et al.* [40]. The uncertainties in the analyzing powers were derived from uncertainties in the phase shifts.

Asymmetries were analyzed on a channel-by-channel basis. A statistical uncertainty of $<2\%$ for the vector polarization was obtained in ≈10 min. Tensor polarization uncertainties were of order 10%. Deuteron polarimetry was performed before and after each $\Delta\sigma$ measurement, and the beam polarization was monitored approximately every 4 h with the TUNL spin-filter polarimeter [41]. Typical deuteron beam polarizations were of the order of $P_i=60\%$ and $P_{ii}=80\%$, where i stands for either y or z.

3. Neutron beam polarization

The neutron beam polarization was calculated from the charged-particle beam polarization using known polarization-transfer coefficients. For the ^{3}H$(\vec{p},\vec{n})^3$He reac-

tion, the neutron beam polarization for the transverse or longitudinal geometries was calculated from the expression

$$P_n(0°) = P_p K_i^{i'}(0°), \tag{21}$$

where $K_i^{i'}(0°)$ are the polarization-transfer coefficients.

An auxiliary measurement of $K_y^{y'}(0°)$ was performed at $E_n = 1.88$ MeV using the Tübingen/TUNL neutron polarimeter [42] calibrated with $n-{}^4$He scattering. The result obtained, $K_y^{y'}(0°) = 0.655 \pm 0.021$, is consistent with the earlier value [$K_y^{y'}(0°) = 0.656 \pm 0.036$] of Wilburn *et al.* [43] measured at $E_n = 1.94$ MeV using the same neutron polarimeter. Since these two results are in excellent agreement and bracket our energy of $E_n = 1.92$ MeV, the present value for $K_y^{y'}(0°)$ was used to calculate $P_n(0°)$.

Values of $K_z^{z'}(0°)$ for the reaction $^3\mathrm{H}(\vec{p},n)^3\mathrm{He}$ were not available below $E_p = 4.0$ MeV ($E_n = 3.2$ MeV). Therefore, auxiliary measurements were performed by Walston *et al.* [44] to determine $K_z^{z'}(0°)$ between 1.3 and 2.8 MeV proton energy.

For the $^2\mathrm{H}(\vec{d},\vec{n})^3\mathrm{He}$ reaction, the neutron beam polarization for the transverse or longitudinal geometries was calculated from the expression [45]

$$P_n = \frac{\frac{3}{2} P_i K_i^{i'}(0°)}{1 + \frac{1}{2} P_{ii} A_{ii}(0°)}. \tag{22}$$

The polarization-transfer coefficient $K_y^{y'}(0°)$ and the tensor analyzing power $A_{yy}(0°)[= -\frac{1}{2} A_{zz}(0°)]$ were extracted from fits to data taken from Lisowski *et al.* [46]. Values for $K_z^{z'}(0°)$ were extracted from Salzman *et al.* [47] and for $A_{zz}(0°)$ from Lisowski *et al.* [46] and Salzman *et al.* [47].

C. Measurements of $P_T x$

The product of proton target polarization and target thickness $P_T x$ was directly measured by low-energy neutron transmission. If $\Delta\sigma_{T(L)}$ is known, Eq. (14) can be rewritten

$$P_T x = \frac{2\epsilon_{T(L)}}{P_n \Delta\sigma_{T(L)}}. \tag{23}$$

At very low energy, $\Delta\sigma_{T(L)}$ is well determined by effective-range expansions, phase-shift analyses, and *NN* potential models. As the neutron energy goes to zero, the tensor interaction turns off and $\Delta\sigma_{T(L)}$ depends only upon the scalar spin-spin interaction, which, at zero energy, only depends on the singlet and triplet $n+p$ scattering lengths $^3S_1$ and $^1S_0$, respectively. As a result, all realistic calculations of $\Delta\sigma_{T(L)}$ agree to high precision at low neutron energies [13].

Therefore, $P_T x$ can be determined from measurements of P_n and the low-energy transmission asymmetry. These measurements were performed for three targets used during the course of our $\Delta\sigma_T$ and $\Delta\sigma_L$ experiments. Neutron transmission asymmetries were measured at $E_n = 1.915$ MeV (transverse) and $E_n = 0.793$ MeV (longitudinal). The neutron beam energy was calibrated using ^{12}C resonances in neutron transmission experiments.

TABLE I. Experimental values of $\Delta\sigma_L$, $\Delta\sigma_T$, and Δ, and ε_1 results of the χ^2 minimization of $\Delta_{calc} - \Delta_{exp}$. The data for $\Delta\sigma_T$ at $E_n = 4.98$ and 7.43 MeV are from Wilburn *et al.* [21]. All other data are from the present work.

E_n (MeV)	$\Delta\sigma_L$ (mb)	$\Delta\sigma_T$ (mb)	Δ (mb)	ε_1 (°)
4.98	94.0±10.8	41.0±33.8	53.0±35.5	0.38±0.26
7.43	−13.4±1.8[a]	−129.0±11.9	115.6±12.0	1.16±0.12
10.7	−42.2±5.9	−140.4±7.0	98.2±9.2	1.35±0.13
14.6	−51.5±4.6	−143.0±7.2	92.5±8.5	1.69±0.16
17.1	−39.9±6.6	−123.9±6.7	84.0±9.4	1.81±0.21
19.7	−32.8±7.2			2.10±0.27

[a]This value was measured at 6.95 MeV and scaled to 7.43 MeV according to the energy dependence of the Nijmegen partial-wave PWA93 analysis.

The average values for $\Delta\sigma_{T(L)}$ using phase-shift analyses and potential models are 940 (3476) mb with a ±2 (±8) mb standard deviation. Our determination of $P_T x$ for the transverse and longitudinal geometries were accurate to 4 and 6 %, respectively. NMR measurements were used to account for the less than 1% differences in target polarization occuring in the interval between $P_T x$ and $\Delta\sigma$ measurements.

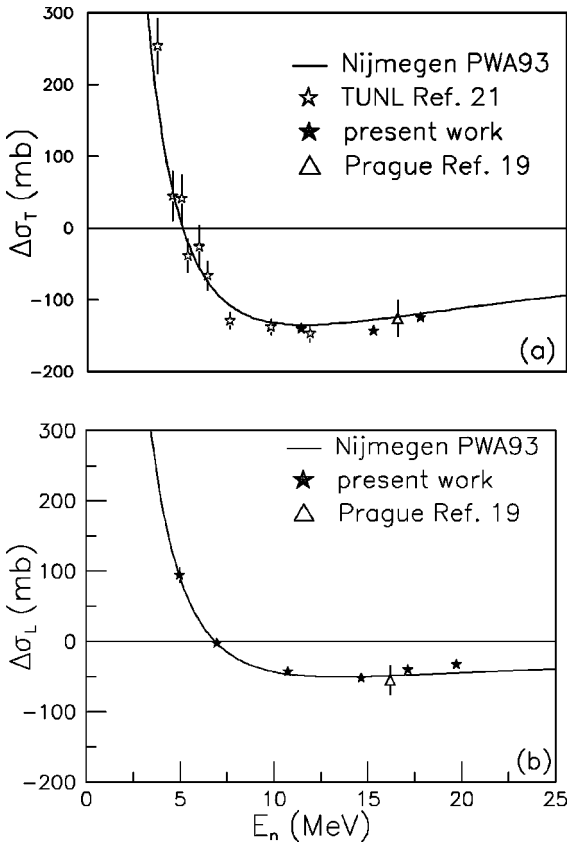

FIG. 8. Plot of experimental values of $\Delta\sigma_T$ (a) and $\Delta\sigma_L$ (b) from the present work and from other measurements. Error bars include statistical and systematic uncertainties.

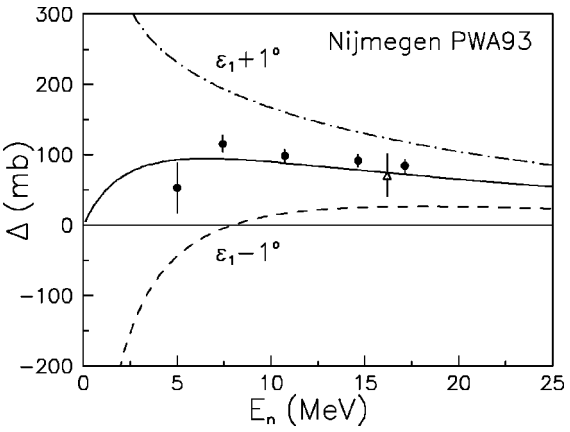

FIG. 9. TUNL results for the observable Δ (filled circles). The error bars include statistical and systematic uncertainties. The datum at $E_n=16.2$ MeV (triangle) was obtained recently at Prague. The curves show the sensitivity of Δ to changes in ε_1: The solid curve is the PWA93 prediction of Δ, and the dot-dashed (dashed) curve is the predicted value of Δ with ε_1 varied by $+1°$ $(-1°)$.

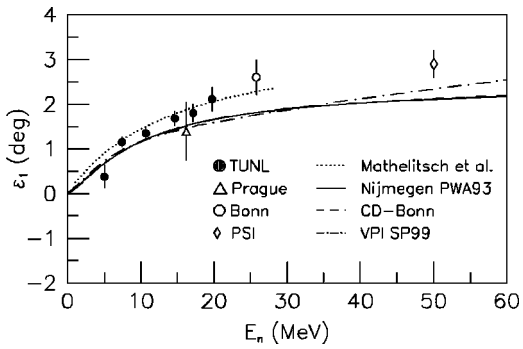

FIG. 10. ε_1 data including new TUNL experimental results (filled circles) and the datum at $E_n=16.2$ MeV (triangle) from Prague. See text for references. Theoretical curves are explained in the text.

V. RESULTS

Following Eq. (14), and using measurements of neutron asymmetries, neutron beam polarizations, and $P_T x$ values, the cross-section differences $\Delta\sigma_T$, $\Delta\sigma_L$, and the difference Δ were calculated. They are listed in Table I. The uncertainties include all statistical and systematic uncertainties added in quadrature. The experimental values for $\Delta\sigma_L$ and $\Delta\sigma_T$ are plotted in Fig. 8 in comparison with the Nijmegen PWA93 prediction. The results for the observable Δ are given in Fig. 9.

The phase shift ε_1 was determined from a single-energy, single-parameter χ^2 minimization of $(\Delta_{calc}-\Delta_{exp})$ at each energy. Δ_{calc} was calculated from trial values of ε_1 and the remaining phase shifts were taken from PWA93. Using this procedure, the description of the cross section and analyzing power data used in PWA93 remains virtually unchanged. The uncertainties associated with the triplet $n+p$ phase shifts given in Eq. (17) have a negligible influence on the overall uncertainty of ε_1. A 1% change in $^3S_1$ at $E_n=10$ MeV changes the difference Δ by only 0.3%. Modifications of the ^3P_j phase-shift parameters that are consistent with the description of the *NN* analyzing power data result in changes of Δ by only 0.1%. Finally, a 5% change of $^3D_1$ affects Δ by 0.25%. This extremely small dependence of Δ on the triplet phase-shift parameters of Eq. (17) is an additional and unique advantage of our approach compared to earlier determinations of ε_1.

Results of this χ^2 minimization are listed in Table I and plotted in Fig. 10. The value at $E_n=19.7$ MeV is from a χ^2 minimization of $\Delta\sigma_L$ alone. The error bars include statistical and systematic uncertainties.

VI. DISCUSSION

Figure 10 compares experimental determinations of ε_1 with theoretical predictions. Here, we omitted the two data points of the Erlangen/Tübingen and Bonn groups near $E_n=15$ MeV (see Fig. 1), which must be plagued by unknown experimental effects. Our data (filled circles) obtained in the energy range below $E_n=20$ MeV support the trend indicated by the previous measurements at 25.6 and 50 MeV. Clearly, the experimental results for ε_1 are substantially higher in magnitude than the phase-shift prediction PWA93 (solid curve) of the Nijmegen group as well as the recent analysis SP99 (dashed-dotted curve) of the VPI group [49]. For completeness, we added in Fig. 10 the prediction of the CD-Bonn potential (dashed curve) as an example for one of the recent high-precision *NN* potential models.

How significant are these larger values for ε_1 for our understanding of *NN* potential models? Since the *NN* tensor force is due mainly to OPE- and ρ-exchange contributions, the answer to this question is not simple. First, it may be helpful to point out that our data are in fair agreement with the effective-range parametrization of Mathelitsch and VerWest [48] (dotted curve in Fig. 10). This parametrization is based on OPE, but here the OPE tensor force is not reduced by invoking a πNN form factor, as is customary in phase-shift analyses and potential models. Furthermore, as has been pointed out by Machleidt [50], our data for ε_1 and the deuteron properties can be reproduced well by an OPE potential with Bonn-B or CD-Bonn type πNN form factor (1.7 GeV), i.e., by a model that does not incorporate any heavier meson-exchange contributions. This observation may point to deficiencies in the theoretical treatment of heavier meson exchange (like ρ, ω, σ, η, and δ exchange) in *NN* potential models. Clearly, ρ exchange has the most important influence in our energy range. However, as pointed out already in the Introduction, it is well known that a strong ρ coupling ($\kappa_\rho=6.1$) is required to fit the $^3P_0$, $^3P_2$, and $^1D_2$ *NN* phase shifts at energies above 100 MeV, where short-range effects are clearly important. Obviously, a mechanism is needed that generates a larger *NN* tensor force and at the same time provides a good fit to the phase-shift parameter referred to above. Interestingly, the description of the low-energy nucleon-nucleon analyzing power $A_y(\theta)$ data, which is sensitive to the ^3P_J *NN* interactions, could tolerate a weak ρ coupling. Finally, as pointed out by Machleidt [50], our data favor a large η for the deuteron *D*- to *S*-state asymptotic normalization constant. In fact, the dotted curve in Fig. 10 is

based on $\eta = 0.0272$. Although larger values for η in general imply larger values for ε_1, this correlation is not very strong.

VII. CONCLUSION

In summary, we have performed polarized neutron beam-polarized proton target transmission experiments below $E_n = 20$ MeV to determine the difference Δ of the spin-dependent $n+p$ total cross-section differences $\Delta\sigma_L$ and $\Delta\sigma_T$. This observable allows for a practically model insensitive determination of the phase-shift parameter ε_1, which is a measure of the $n+p$ tensor interaction at low and intermediate energies. In combination with other experiments, our values of ε_1 support a *NN* tensor interaction that is stronger than predicted by all modern meson-exchange based *NN* potential models and the Nijmengen PWA93 and VPI SP99 phase-shift analyses. This finding has far reaching consequences with respect to the binding of few-nucleon systems. Following the traditional approach, it calls for larger three-nucleon force effects than currently considered and expected from the analysis of three-nucleon data.

Clearly, our high-accuracy data for ε_1 raise more questions than they provide answers. One of the unanswered questions is whether the persistent difficulties experienced with current *NN* potential models in reproducing the electric quadrupole moment of the deuteron is related to our findings for ε_1. However, our data add significantly to the conjecture that new concepts are needed to provide a more fundamental and accurate description of the *NN* interaction than presently available.

ACKNOWLEDGMENTS

We gratefully acknowledge the support of the U.S. Department of Energy, Office of High Energy and Nuclear Physics, under Grants No. DE-FG02-97ER41042 and DE-FG02-97ER41033. Correspondence and discussions with Professor R. Machleidt and Professor I. I. Strakovsky are greatly appreciated. Finally, we acknowledge the support of the Robert A. Welch Foundation.

[1] V. G. J. Stoks, R. A. M. Klomp, C. P. F. Terheggen, and J. J. de Swart, Phys. Rev. C **49**, 2950 (1994).
[2] R. B. Wiringa, V. G. J. Stoks, and R. Schiavilla, Phys. Rev. C **51**, 38 (1995).
[3] R. Machleidt, F. Sammarruca, and Y. Song, Phys. Rev. C **53**, R1483 (1996).
[4] V. G. J. Stoks, R. A. M. Klomp, M. C. M. Rentmeester, and J. J. de Swart, Phys. Rev. C **48**, 792 (1993).
[5] D. Plümper, J. Fender, and M. F. Gari, Phys. Rev. C **49**, 2370 (1994).
[6] A. Kievsky, S. Rosati, W. Tornow, and M. Viviani, Nucl. Phys. **A607**, 402 (1996).
[7] V. I. Kukulin, V. N. Pomerantsev, A. Faessler, A. J. Buchmann, and E. M. Tursunov, Phys. Rev. C **57**, 535 (1998).
[8] A. Valcarce, A. Buchmann, F. Fernandez, and A. Faessler, Phys. Rev. C **50**, 2246 (1994).
[9] S. Weinberg, Phys. Lett. B **251**, 288 (1990).
[10] D. B. Kaplan, M. S. Savage, and M. B. Wise, Phys. Lett. B **424**, 390 (1998); Nucl. Phys. **B534**, 329 (1998).
[11] E. Epelbaoum, W. Glöckle, A. Krüger, and U. G. Meissner, Nucl. Phys. **A645**, 413 (1999).
[12] G. E. Brown and R. Machleidt, Phys. Rev. C **50**, 1731 (1994).
[13] B. W. Raichle, C. R. Gould, D. G. Haase, M. L. Seely, J. R. Walston, W. Tornow, W. S. Wilburn, S. I. Penttilä, and G. W. Hoffmann, Phys. Rev. Lett. **83**, 2711 (1999).
[14] R. Henneck, Phys. Rev. C **47**, 1859 (1993).
[15] M. Ockenfels, F. Meyer, T. Köble, W. von Witsch, J. Weltze, K. Wingender, and G. Wollmann, Nucl. Phys. **A526**, 109 (1991).
[16] M. Ockenfels, T. Köble, M. Schwindt, J. Weltze, and W. von Witsch, Nucl. Phys. **A534**, 248 (1991).
[17] M. Schöberl, H. Kuiper, R. Schmelzer, G. Mertens, and W. Tornow, Nucl. Phys. **A489**, 284 (1988).
[18] P. Clotten, P. Hempen, K. Hofenbitzer, V. Huhn, W. Metschulat, M. Schwindt, L. Wätzold, Ch. Weber, and W. von Witsch, Phys. Rev. C **58**, 1325 (1998).
[19] J. Brož *et al.*, Z. Phys. A **354**, 401 (1996).
[20] J. Brož *et al.*, Z. Phys. A **359**, 23 (1997).
[21] W. S. Wilburn, C. R. Gould, D. G. Haase, P. R. Huffman, C. D. Keith, N. R. Roberson, and W. Tornow, Phys. Rev. C **52**, 2351 (1995).
[22] R. Machleidt, Adv. Nucl. Phys. **19**, 175 (1989).
[23] R. A. Arndt, C. H. Oh, I. I. Strakovsky, R. L. Workman, and F. Dohrmann, Phys. Rev. C **56**, 3005 (1997).
[24] P. Doll, V. Eberhard, G. Fink, R.W. Finlay, T.D. Ford, W. Heeringa, O. Klages, H. Krupp, and Chr. Wölfl, in *Few Body XII*, edited by B.K. Jennings (TRIUMF, Vancouver, 1989), p. C16.
[25] R. J. N. Phillips, Nucl. Phys. **43**, 413 (1963).
[26] V. Hnizdo, Phys. Rev. C **50**, 2639 (1994).
[27] V. Hnizdo (private communication).
[28] W. Tornow, O. K. Baker, C. R. Gould, D. G. Haase, N. R. Roberson, and W. S. Wilburn, in *Physics with Polarized Beams and Polarized Targets*, edited by J. Sowinski and S. E. Vigdor (World Scientific, Singapore, 1989).
[29] A. Abragam, *Principles of Nuclear Magnetism* (Oxford University Press, Oxford, 1961).
[30] M. Krumpolc and J. Roček, J. Am. Chem. Soc. **101**, 3206 (1979).
[31] B. van den Brandt, J. A. Konter, and S. Mango, Nucl. Instrum. Methods Phys. Res. A **289**, 526 (1990).
[32] G. R. Court, D. W. Gifford, P. Harrison, W. G. Heyes, and M. A. Houlden, Nucl. Instrum. Methods Phys. Res. A **324**, 433 (1993).
[33] T. B. Clegg, H. J. Karwowski, S. K. Lemieux, R. W. Sayer, E. R. Crosson, W. M. Hooke, C. R. Howell, H. W. Lewis, A. W. Lovette, H. J. Pfutzner, K. A. Sweeton, and W. S. Wilburn, Nucl. Instrum. Methods Phys. Res. A **357**, 200 (1995).

[34] J. R. Walston, Ph.D. thesis, North Carolina State University, 1999.
[35] B. W. Raichle, C. R. Gould, D. G. Haase, M. L. Seely, J. R. Walston, W. Tornow, W. S. Wilburn, G. W. Hoffmann, and S. I. Penttilä, in *Application of Accelerators in Research and Industry*, edited by J. L. Duggan and I. L. Morgan, AIP Conf. Proc. No. 475 (AIP, Woodbury, NY, 1999), p. 223.
[36] J. E. Koster, Ph.D. thesis, North Carolina State University, 1990.
[37] B. W. Raichle, Ph. D. thesis, North Carolina State University, 1997.
[38] G. R. Satchler, *Direct Nuclear Reactions* (Oxford University Press, Oxford, 1983).
[39] P. Schwandt, T. B. Clegg, and W. Haeberli, Nucl. Phys. **A163**, 432 (1971).
[40] M. Bittcher, W. Grüebler, V. König, P. A. Schmelzbach, B. Vuaridel, and J. Ulbricht, Few-Body Syst. **9**, 165 (1990).
[41] A. J. Mendez, C. D. Roper, J. D. Dunham, and T. B. Clegg, Rev. Sci. Instrum. **67**, 3073 (1996).
[42] W. Tornow, Z. Phys. **266**, 357 (1974).
[43] W. S. Wilburn, C. R. Gould, G. M. Hale, P. R. Huffman, C. D. Keith, N. R. Roberson, and W. Tornow, Few-Body Syst. **24**, 27 (1998).
[44] J. R. Walston, C. D. Keith, C. R. Gould, D. G. Haase, B. W. Raichle, M. L. Seely, W. Tornow, W. S. Wilburn, G. W. Hoffmann, and S. I. Penttilä, Phys. Rev. C **58**, 1314 (1998).
[45] G. G. Ohlsen, Rep. Prog. Phys. **35**, 717 (1972).
[46] P. W. Lisowski, R. L. Walter, C. E. Bush, and T. B. Clegg, Nucl. Phys. **A242**, 298 (1975).
[47] G. C. Salzman, J. C. Martin, J. J. Jarmer, J. E. Simmons, G. G. Ohlsen, and T. R. Donoghue, Phys. Lett. **45B**, 123 (1973).
[48] L. Mathelitsch and B. J. VerWest, Phys. Rev. C **29**, 739 (1994).
[49] I. I. Strakovsky (private communication).
[50] R. Machleidt (private communication).